JOURNAL OF SPACECRAFT AND ROCKETS
Vol. 38, No. 2, March–April 2001

Solar Sail Orbit Operations at Asteroids

Esther Morrow*
University of California, San Diego, La Jolla, California 92093-0214
D. J. Scheeres†
University of Michigan, Ann Arbor, Michigan 48109-2140
and
Dan Lubin‡
University of California, San Diego, La Jolla, California 92093-0221

The inherent capabilities of solar sails and that they need no onboard supplies of fuel for propulsion make them well suited for use in long-term, multiple-objective missions. They are especially well suited for the exploration of asteroids, where one spacecraft could rendezvous with a number of asteroids in succession. The orbital mechanics of solar sail operations about an asteroid, however, have not yet been studied in detail. Building on previous studies, we find both hovering points and orbiting trajectories about various sized asteroids using equations of motion for a solar sail spacecraft. The orbiting trajectories are stable and offer good coverage of the asteroid surface, although restrictions on sail acceleration are needed for smaller asteroids.

Nomenclature

$\boldsymbol{a}$	=	solar radiation pressure acceleration vector
a_p	=	sail acceleration, mm/s^2
$\tilde{a}_p$	=	normalized sail acceleration, $a_p/(\mu r_H^{-2})$
a_{p_0}	=	sail acceleration at 1 AU or characteristic acceleration, mm/s^2
$a_{p_0}^M$	=	maximum sail acceleration for feasible orbit operations, mm/s^2
$a_{p_0}^m$	=	minimum sail acceleration for feasible orbit operations, mm/s^2
$a_{\rm sc}$	=	spacecraft orbit semimajor axis, km
$\tilde{a}_{\rm sc}$	=	normalized spacecraft orbit semimajor axis, $a_{\rm sc}/r_0$
c	=	speed of light, 3×10^8 m/s
e	=	spacecraft orbit eccentricity
$\boldsymbol{e}$	=	spacecraft periapsis vector
$\boldsymbol{H}$	=	spacecraft angular momentum vector
i	=	spacecraft orbit inclination, deg
$\boldsymbol{l}$	=	incoming sunlight unit vector
N	=	angle proportional to asteroid true anomaly about sun, $\sim nt/\cos\gamma$
n	=	asteroid mean motion about sun
$\boldsymbol{n}$	=	unit normal vector to spacecraft
P	=	orbit parameter of asteroid
R	=	radial distance of asteroid from sun, km
$\tilde{R}$	=	radial distance of asteroid from sun, AU
R_0	=	1 AU measured in km, 1.5×10^8 km
r	=	radial distance of spacecraft from asteroid, km
$\boldsymbol{r}$	=	radius vector from asteroid to spacecraft
r_H	=	Hill radius, km
r_n	=	nondimensionalized value of r, r/r_H
r_0	=	mean asteroid radius, km
t	=	time, s
W/R_0^2	=	solar radiation intensity, 1368 W/m^2 at 1 AU
x, y, z	=	position coordinates in the rotating frame, km
$\boldsymbol{x}, \boldsymbol{y}, \boldsymbol{z}$	=	coordinate vectors in the rotating frame
x_n, y_n, z_n	=	normalized position coordinates
α	=	spacecraft pitch angle
β	=	nondimensional sail loading parameter or sail lightness number
γ	=	perturbation angle
θ	=	spacecraft declination angle measured from asteroid
μ	=	asteroid gravitational parameter, km^3/s^2
$\mu_{\rm sun}$	=	sun gravitational parameter, $\sim 1.34 \times 10^{11}$ km^3/s^2
ν, ν_0	=	spacecraft orbit true anomaly, deg
σ	=	sail mass to area ratio or sail loading, kg/m^2
σ^*	=	critical sail loading parameter, 1.53 g/m^2
ϕ	=	spacecraft yaw angle
ψ	=	spacecraft right ascension angle measured from asteroid
Ω	=	magnitude of angular velocity vector, $\Omega = \sqrt{(\mu_{\rm sun}/a_{\rm ast}^3)}$ s^{-1}
$\boldsymbol{\Omega}$	=	angular velocity vector
$\tilde{\Omega}, \tilde{\Omega}_0$	=	spacecraft orbit longitude of the ascending node relative to the sun–asteroid line, deg
ω	=	spacecraft orbit argument of periapsis, deg
$(\dot{}), (\ddot{})$	=	first and second time derivatives, respectively

Introduction

THE concept of the solar sail has been known for more than a century, but it has only been with the advent of microtechnologies and thin films that solar sailing appears to be a practical mode of spaceflight.[1] Because of the long history and proven usefulness of conventional spacecraft, solar sails will never be considered as a replacement technology for conventional propulsion; however, there are some mission applications for which sails are particularly well suited. A long-term, multiple-objective mission such as one to more than one asteroid is just such an application. These missions have not yet been studied in detail, and, in particular, solar sail behavior about asteroids has not been studied. This paper is a first step in this direction.

Relying on solar propulsion instead of convential propulsion allows us flexibility in studying asteroids. With a solar sail spacecraft, we are not limited by carrying onboard supplies of fuel for propulsion. Depending on sail performance in the space environment, several asteroids could be visited in succession and orbited for extended periods of time. Thus, a spacecraft of this type could enhance our understanding of asteroids by shortening the period of time between missions.

We derive a model for solar sail dynamics about an asteroid and consider a number of possible options for operations in the asteroid environment. We find limits on feasible sail operations as a function of sail parameters, asteroid parameters, and asteroid orbit. Both orbital and hovering options are considered. For the purposes of

Received 7 July 2000; revision received 17 November 2000; accepted for publication 22 November 2000.

*Research Associate, California Space Institute, Scripps Institute of Oceanograpy 0214; esther@arcane.ucsd.edu. Member AIAA.

†Assistant Professor, Department of Aerospace Engineering; scheeres@umich.edu. Member AIAA.

‡Associate Research Physicist, California Space Institute, Scripps Institute of Oceanography 0221; dlubin@ucsd.edu.

this study, we focus only on the behavior of the solar sail spacecraft after rendezvous has been achieved.

For our model we assume a spherical, point mass asteroid, a perfectly reflecting solar sail, and a circular asteroid orbit about the sun. These assumptions can be relaxed in future studies. We first develop the basic equations of motion for the system. We then consider the constraints and feasibility of hovering sail trajectories, complementing the studies made by McInnes et al.[2] and McInnes.[3] We find a continuum of hovering points that would allow station keeping to monitor the asteroid at a particular phase angle for extended periods of time. Next, we consider the constraints and feasibility of orbital operations about an asteroid, from which we develop a number of basic criteria for necessary sail acceleration as a function of asteroid parameters. The orbital trajectories are found to be stable and to offer good coverage of the asteroid surface. These trajectories would be very useful for mapping purposes.

Model

To model the dynamics of a sail close to an asteroid we can apply the Hill approximation with appropriate generalizations to account for the solar sail's force vector. The Hill approximation applies very well to the motion of spacecraft about asteroids, due to the small mass of asteroids relative to the sun and due to the proximity that the craft maintains to the asteroid.[4] The Hill approximation can also be easily modified to account for the effect of solar radiation pressure, leading to the equations of motion[5]:

$$\ddot{x} - 2\Omega\dot{y} = -(\mu/r^3)x + 3\Omega^2 x + a_x \tag{1}$$

$$\ddot{y} + 2\Omega\dot{x} = -(\mu/r^3)y + a_y \tag{2}$$

$$\ddot{z} = -(\mu/r^3)z - \Omega^2 z + a_z \tag{3}$$

where the origin of the rotating reference frame is centered at the asteroid with the positive x axis in the antisolar direction, the z axis normal to the asteroid orbit ecliptic, and the y axis according to the right-hand rule. This frame rotates about the z axis with angular velocity $\Omega = \sqrt{(\mu_{\text{sun}}/a_{\text{ast}}^3)}$, where μ_{sun} is the sun's gravitational parameter and a_{ast} is the asteroid's heliocentric orbit radius in kilometers. The gravitational parameter of the asteroid is denoted as μ.

The spacecraft is propelled by solar radiation flux incident on the sail, which is herein assumed to be perfectly reflecting and planar. The sail receives an action force from incident sunlight and a reaction force from the reflected light, so that the net force is directed normal to the surface of the sail and pointing away from the sun. The acceleration vector of this force is denoted as $\boldsymbol{a} = [a_x \;\; a_y \;\; a_z] = a_p(\boldsymbol{l}\cdot\boldsymbol{n})^2\boldsymbol{n}$.

The unit vector $\boldsymbol{l}$ defines the direction of the incident light, and $\boldsymbol{n}$ is the unit normal to the sail. In the rotating reference frame, $\boldsymbol{l}$ will always equal [1 0 0], and $\boldsymbol{n}$ will be $[\cos\phi\cos\alpha \;\; \sin\phi\cos\alpha \;\; \sin\alpha]$, where α is the sail pitch angle with respect to the sun line and ϕ is the orientation angle about the z axis as shown in Fig. 1. The direction of the solar radiation pressure (SRP) force can never be pointed toward the sun, and so the sail attitude is constrained such that $\boldsymbol{l}\cdot\boldsymbol{n} \geq 0$.

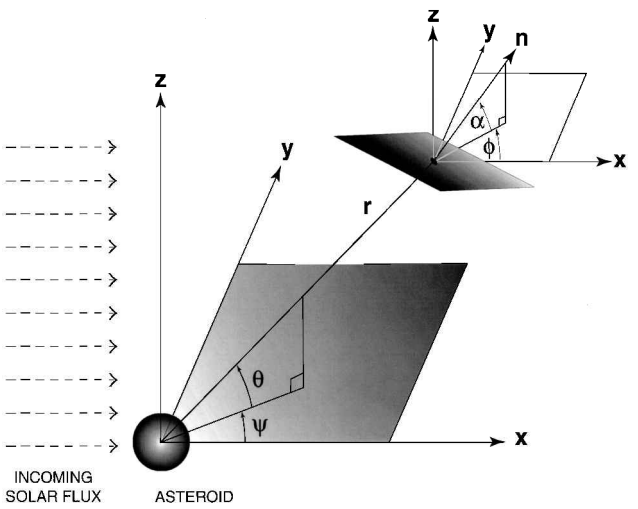

Fig. 1 Model schematic for a solar sail spacecraft about an asteroid.

The parameter a_p is called the sail acceleration and is represented as

$$a_p = \left(2W/cR_0^2\right)\left(R_0^2/R^2\right)(1/\sigma) \tag{4}$$

for a perfectly reflecting solar sail where W/R_0^2 is the solar radiation intensity, c is the speed of light, R_0 is the distance from the sun to the Earth, R is the distance from the sun to the sail in kilometers, and σ is the mass to area ratio of the sail or sail loading. For a nonperfect sail, there will be an additional component of acceleration transverse to the sail normal. At 1 AU

$$a_p = a_{p_0} = \left(2W/cR_0^2\right)(1/\sigma) \tag{5}$$

and, in general,

$$a_p = a_{p_0}\left(R_0^2/R^2\right) \tag{6}$$

Thus, SRP varies as $1/R^2$ about the sun (but see discussion by McInnes[1]).

Multiplying and dividing by the sun's gravitational parameter μ_{sun}, we have

$$a_p = (2W/c\mu_{\text{sun}})\left(\mu_{\text{sun}}/R^2\right)(1/\sigma) \tag{7}$$

or

$$a_p = \beta\left(\mu_{\text{sun}}/R^2\right) \tag{8}$$

where $\beta = \sigma^*/\sigma$ is the nondimensional sail loading parameter, called the sail lightness number, defined to be the ratio of the SRP acceleration to the solar gravitational acceleration. The critical sail loading parameter $\sigma^* = 2W/c\mu_{\text{sun}}$ is a constant whose value is approximately 1.53 g/m^2.

The value of the sail acceleration varies with both the efficiency and size of the sail.[1] For example, McInnes[1] shows that a typical value for a 98 × 98 m square sail that carries a payload of 25 kg is 1 mm/s^2. At this acceleration, a solar sail spacecraft has trip times to asteroids comparable to conventional spacecraft. This spacecraft design yields a sail loading parameter of 9.12 g/m^2, or a sail lightness number of 0.1678. This parameter can be reached with a sail film thickness of 2 μm.

Solar Sail Hovering Constraints and Dynamics

Given the basic equations of motion, we search for conditions under which the spacecraft can be placed into an artificial equilibrium point, found by setting all of the time derivatives to zero and finding the combination of SRP acceleration and natural forces that will yield no net acceleration acting on the sail. The result is a specialization of the analysis carried out by McInnes[2] for the restricted three-body problem, now applied to the Hill problem. Following the Hill equations, we find the equations of motion of a solar sail spacecraft to be as in Eqs. (1–3).

Because the sail normal is required to point in the antisolar direction, we are limited to $-\pi/2 \leq \alpha \leq \pi/2$. The problem is symmetric about the angle $\alpha = 0$, however, and so we need only consider $0 \leq \alpha \leq \pi/2$. When $\alpha = \pi/2$ the sail is edge on to the sun. In this situation, we effectively are in irons, that is, we have no SRP force at all. Although there may be instances when this effect would be desirable, we do not consider this case explicitly. Thus, we limit our discussion to $0 \leq \alpha < \pi/2$.

Likewise, to satisfy the constraint $\boldsymbol{l}\cdot\boldsymbol{n} \geq 0$, we only consider ϕ limited to $-\pi/2 \leq \phi \leq \pi/2$. The problem is also symmetric about $\phi = 0$; therefore, we consider ϕ such that $0 \leq \phi < \pi/2$ for the same reasons stated for α.

The preceding definitions lead us, in the most general case, to define the equilibrium equations for hovering points to be

$$0 = -(\mu/r^3)x + 3\Omega^2 x + a_x \tag{9}$$

$$0 = -(\mu/r^3)y + a_y \tag{10}$$

$$0 = -(\mu/r^3)z - \Omega^2 z + a_z \tag{11}$$

with the components of $\boldsymbol{a}$ as

$$a_x = a_p \cos^2\phi \cos^2\alpha \cos\phi \cos\alpha \tag{12}$$

$$a_y = a_p \cos^2\phi \cos^2\alpha \sin\phi \cos\alpha \tag{13}$$

$$a_z = a_p \cos^2\phi \cos^2\alpha \sin\alpha \tag{14}$$

and the vector $\boldsymbol{r}$ as

$$\boldsymbol{r} = r[\cos\theta\cos\psi \quad \cos\theta\sin\psi \quad \sin\theta] \tag{15}$$

where θ is the declination angle measured from the xy plane toward the z axis and ψ is the right ascension angle measured in the xy plane from the $+x$ axis, as shown in Fig. 1.

Hovering Points with No SRP Force

We first consider the hovering points for the system with no SRP force. In this case, $a_x = a_y = a_z = 0$. It is obvious that y and z must also be 0 to satisfy Eqs. (10) and (11), respectively. Thus, from Eq. (9), $\mu/r^3 = 3\Omega^2$ at equilibrium. Solving for r, we find

$$r = (\mu/3\Omega^2)^{\frac{1}{3}} \tag{16}$$

This value is called the Hill radius and denoted r_H herein. We use this radius to normalize the hovering point radii throughout our analysis.

Hovering Points Along the *x* Axis

We consider next the simplest situation for the model, when the sail is along the x axis. Here, ϕ, ψ, and α are all 0 because there are no components in the y or z directions. In this case, the equations of motion become

$$0 = -(\mu/r^3)x + 3\Omega^2 x + a_p \tag{17}$$

which becomes

$$x/|x|^3 = (a_p/\mu)\left[1\Big/\left(1 - r_n^3\right)\right] \tag{18}$$

where r_n is the nondimensionalized value for r normalized by the Hill radius r_H, that is, $r_n = r/r_H$.

In this case there are two equilibrium points, one for x positive and one for x negative. When x is positive, that is, on the asteroid night side, r_n must be less than 1, which means that the hovering radius is less than the Hill radius. When x is negative (on the asteroid day side), r_n must be greater than 1, which means that the hovering radius is greater than the Hill radius.

Hovering Points in the *xz* Plane

Now consider when the sail is in the xz plane. Here, ϕ and ψ are both 0 whereas α varies from 0 to $\pi/2$ as discussed. In this case, the equations of motion are as in Eqs. (9–11), where

$$a_x = a_p \cos^2\alpha \cos\alpha \tag{19}$$

$$a_y = 0 \tag{20}$$

$$a_z = a_p \cos^2\alpha \sin\alpha \tag{21}$$

We see immediately that y must be 0 from Eq. (10).

Letting $x = r\cos\theta$ and $z = r\sin\theta$, we can solve for angle α and a_p in terms of r and θ. When we rewrite Eqs. (9) and (11), they become

$$(\mu/r^3 - 3\Omega^2) r\cos\theta = a_p \cos^2\alpha \cos\alpha \tag{22}$$

$$(\mu/r^3 + \Omega^2) r\sin\theta = a_p \cos^2\alpha \sin\alpha \tag{23}$$

which gives

$$\tan\alpha = \left[\frac{\mu/r^3 + \Omega^2}{\mu/r^3 - 3\Omega^2}\right]\tan\theta \tag{24}$$

Multiplying the numerator and denominator by $3r^3/\mu$, we have

$$\tan\alpha = \left(\frac{1 + \frac{1}{3}r_n^3}{1 - r_n^3}\right)\tan\theta \tag{25}$$

which gives the sail orientation as a function of sail position.

When we use the identity $\sec^2\alpha = 1 + \tan^2\alpha$, Eq. (9) becomes

$$(\mu/r^2)\left(1 - r_n^3\right)\cos\theta = a_p(1 + \tan^2\alpha)^{-\frac{3}{2}} \tag{26}$$

and, substituting in Eq. (25) and solving for a_p, we have

$$a_p = \left[\mu\Big/r^2\left(1 - r_n^3\right)^2 \cos^2\theta\right]\left[\left(1 - r_n^3\right)^2 + \tfrac{8}{3}r_n^3 \sin^2\theta\left(1 - \tfrac{1}{3}r_n^3\right)\right]^{\frac{3}{2}} \tag{27}$$

which gives the necessary sail acceleration as a function of sail position. We can normalize a_p by dividing by μ/r_H^2. We then find

$$\tilde{a}_p = a_p\Big/\left(\mu/r_H^2\right) \tag{28}$$

$$\tilde{a}_p = \left[1\Big/r_n^2\left(1 - r_n^3\right)^2 \cos^2\theta\right]\left[\left(1 - r_n^3\right)^2 + \tfrac{8}{3}r_n^3 \sin^2\theta\left(1 - \tfrac{1}{3}r_n^3\right)\right]^{\frac{3}{2}} \tag{29}$$

$$\tilde{a}_p = \left[1\Big/x_n^2\left(1 - r_n^3\right)^2\right]\left[\left(1 - r_n^3\right)^2 + \tfrac{8}{3}r_n z_n^2\left(1 - \tfrac{1}{3}r_n^3\right)\right]^{\frac{3}{2}} \tag{30}$$

where $x_n = r_n\cos\theta$ and $z_n = r_n\sin\theta$.

When $r_n \ll 1$ (i.e., the solar sail is close to the asteroid compared to its ideal Hill radius), then

$$\tan\alpha \sim \tan\theta\left(1 + \tfrac{4}{3}r_n^3 + \cdots\right) \tag{31}$$

$$a_p \sim (\mu/r^2\cos^2\theta)\left[1 + (4\sin^2\theta - 1)r_n^3 + \cdots\right] \tag{32}$$

In this case, the perturbation due to the solar tidal terms has a small effect on the motion of the spacecraft and is characterized by the value of r_n^3.

Out-of-Plane Hovering Points

For out-of-plane hovering points, we must take into consideration the most general form of the equations of motion at equilibrium with the equations for SRP and the equation for $\boldsymbol{r}$ as given earlier, namely,

$$0 = -(\mu/r^3)r\cos\theta\cos\psi + 3\Omega^2 r\cos\theta\cos\psi + a_x \tag{33}$$

$$0 = -(\mu/r^3)r\cos\theta\sin\psi + a_y \tag{34}$$

$$0 = -(\mu/r^3)r\sin\theta - \Omega^2 r\sin\theta + a_z \tag{35}$$

with

$$a_x = a_p \cos^2\phi \cos^2\alpha \cos\phi \cos\alpha \tag{36}$$

$$a_y = a_p \cos^2\phi \cos^2\alpha \sin\phi \cos\alpha \tag{37}$$

$$a_z = a_p \cos^2\phi \cos^2\alpha \sin\alpha \tag{38}$$

Dividing Eq. (34) by Eq. (33), we find that

$$\tan\phi = \left[1\Big/\left(1 - r_n^3\right)\right]\tan\psi \tag{39}$$

From this equation, we see that angle ϕ is related to angle ψ alone, which indicates that as the sail moves out of the xz plane it must also turn so that the sail normal is always pointing approximately radially outward from the asteroid.

Next, we want to solve for angle α and a_p as in the last section, and so we again use the identity $1 + \tan^2\phi = \sec^2\phi$ to find that

$$\sec\phi = \left[\frac{\left(1-r_n^3\right)^2 + \tan^2\psi}{\left(1-r_n^3\right)^2}\right]^{\frac{1}{2}} \tag{40}$$

Dividing Eq. (35) by Eq. (33), we arrive at the relation

$$\tan\alpha = \left(1+\tfrac{1}{3}r_n^3\right)\left[\left(1-r_n^3\right)^2 + \tan^2\psi\right]^{-\frac{1}{2}} \sec\psi\tan\theta \tag{41}$$

Solving for a_p from Eq. (33), we have

$$(\mu/r^3 - 3\Omega^2) r\cos\theta\cos\psi = a_p(1+\tan^2\phi)^{-\frac{3}{2}}(1+\tan^2\alpha)^{-\frac{3}{2}} \tag{42}$$

which becomes

$$a_p = \left[\mu/r^2\left(1-r_n^3\right)^2\cos^2\theta\cos^2\psi\right]\left[\left(1-r_n^3\right)^2 + \tfrac{8}{3}r_n^3\sin^2\theta\left(1-\tfrac{1}{3}r_n^3\right) + r_n^3\left(2-r_n^3\right)\sin^2\psi\cos^2\theta\right]^{\frac{3}{2}} \tag{43}$$

and, after normalizing by dividing by μ/r_H^2 as before, we have

$$\tilde{a}_p = \left[1/x_n^2\left(1-r_n^3\right)^2\right]\left[\left(1-r_n^3\right)^2 + \tfrac{8}{3}r_n z_n^2\left(1-\tfrac{1}{3}r_n^3\right) + r_n y_n^2\left(2-r_n^3\right)\right]^{\frac{3}{2}} \tag{44}$$

again giving the sail acceleration and orientation as a function of sail position. In this case, however, we define the normalized position coordinates as $x_n = r_n\cos\theta\cos\psi$, $y_n = r_n\cos\theta\sin\psi$, and $z_n = r_n\sin\theta$.

Once again, when $r_n \ll 1$, we can expand each function about r_n and find

$$\tan\phi \sim \tan\psi\left(1 + r_n^3 + \cdots\right) \tag{45}$$

$$\tan\alpha \sim \tfrac{1}{3}\tan\theta\left[3 + r_n^3(1+3\cos^2\psi) + \cdots\right] \tag{46}$$

$$a_p \sim (\mu/r^2)\sec^2\psi\sec^2\theta\left\{1 + r_n^3[-1 + 3\sin^2\psi + (1+3\cos^2\psi)\sin^2\theta] + \cdots\right\} \tag{47}$$

Notice that when $\psi = 0$, the approximations for $\tan\alpha$ and a_p revert back to those found in the xz plane.

Practical Consideration of the Hovering Points

The existence of these equilibrium points is of interest for scientific missions. One application is to use these points to monitor an asteroid at a constant phase angle for an extended length of time. To implement such a design, however, it is necessary to estimate the normalized sail acceleration $\tilde{a}_p$ before sail construction and launch. Thus, we first look in detail at what parameters are needed to estimate the value of $\tilde{a}_p$ at a given asteroid. In particular, we can show that this value depends only on the sail's acceleration a_{p0} and the asteroid's gravitational parameter and is independent of the asteroid's distance from the sun. We see this by expanding the definition for $\tilde{a}_p$:

$$\tilde{a}_p = a_p/(9\mu\Omega^4)^{\frac{1}{3}} \tag{48}$$

which, when we combine with Eq. (6), gives

$$\tilde{a}_p = \frac{a_{p0}R_0^2}{(9\mu\Omega^4R^6)^{\frac{1}{3}}} \tag{49}$$

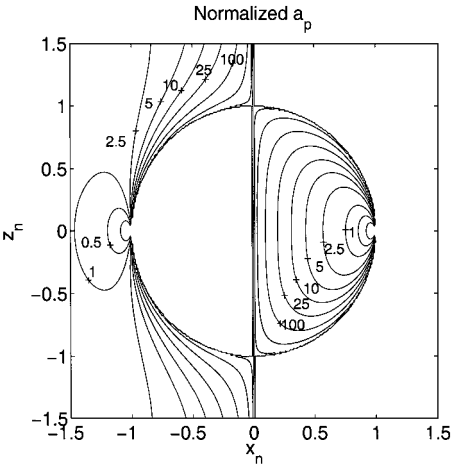

Fig. 2 Spacecraft position contours for different values of $\tilde{a}_p$; all parameters are nondimensionalized.

For an asteroid in a circular orbit, however, we have $\Omega = \sqrt{(\mu_{\text{sun}}/R^3)}$. Therefore, the relation becomes

$$\tilde{a}_p = \frac{a_{p0}R_0^2}{\left(9\mu\mu_{\text{sun}}^2\right)^{\frac{1}{3}}} \tag{50}$$

or, in terms of the sail lightness number from Eq. (8),

$$\tilde{a}_p = \beta(\mu_{\text{sun}}/9\mu)^{\frac{1}{3}} \tag{51}$$

This form of $\tilde{a}_p$ relates the normalized value of a_p to the asteroid mass and the sail's acceleration. Once a target asteroid is identified, its gravitational parameter μ can be constrained by ground-based observations of its size and spectral type (which will put constraints on its density). This estimate may allow sufficient accuracy for preliminary mission planning, incorporating sufficient reserves to cover the likely uncertainty range of the asteroid's mass.

In choosing the sail acceleration parameter, it will be necessary to evaluate the possible hovering positions in the asteroid frame. In the following, we only consider hovering points in the xz-plane, the suitable generalizations can be found for hovering positions out of this plane as well. Figure 2 presents a contour plot of normalized sail acceleration as a function of position in the $x_n z_n$-plane. These results are similar to the contours of sail lightness numbers that McInnes[2] found in the restricted three-body problem, but may have a significantly different form for a nonperfectly reflecting sail.[3] For comparison purposes, the asteroids that we use for this paper have $\tilde{a}_p$ values of approximately 170 for Vesta, 533 for Eros, and 1331 for Ida with corresponding β values of 0.1686, 0.0169, and 0.0843, respectively.

A sail with a given sail acceleration (which is transformed into $\tilde{a}_p$ at a given asteroid) can ideally move along lines of constant contour by modifying the orientation of the sail. Thus, the line of constant $\tilde{a}_p$ defines the hovering positions that a sail can have at an asteroid. McInnes[2] determined that all such hovering points were unstable in the Lyapunov sense, but were controllable using feedback control to sail attitude alone (see also McInnes[6]). Instability and controllability can be established similarly here because McInnes's[2] results satisfied equations that took into account a general form for the potential.

In planning multiple-objective missions to asteroids, it would be best to determine the sail acceleration necessary for the desired radial distance from the largest asteroid first. Once the maximum sail acceleration is chosen, nothing can be done to increase it short of ejecting mass. At the same time, the necessary sail acceleration at the smallest target asteroid must be considered to design a useful hovering position at that body. In general, we see from Fig. 2 that for large values of $\tilde{a}_p$ (which can correspond to small asteroids) it is always possible to find a hovering position that corresponds to that larger value. In general, the sail will be forced to hover out of the asteroid orbital plane (i.e., at nonzero values of z_n) to also

Table 1 Asteroid parameters, maximum and minimum sail accelerations, and normalization factors for asteroids Vesta, Eros, and Ida

Asteroid	r_0, km	r_H, km	μ, km^3/s^2	$\tilde{R}$, AU	a^M_{p0}, mm/s^2	a^m_{p0}, mm/s^2	μ/r_H^2, mm/s^2
Vesta	244.27	116,680	14.2568	2.36	83.17	0.0494	0.0105
Eros	8.87	2,308	0.0005	1.46	0.79	0.0012	0.0009
Ida	15.65	9,064	0.0038	2.86	7.83	0.0035	0.0005

ensure that its hovering radius is sufficiently large as compared to the asteroid's radius.

Finally, we discuss some particulars of the contour plot in Fig. 2. First we focus on the asteroid night side ($0 \le \theta < \pi/2$). From Eq. (30), we see that it takes an infinitely large $\tilde{a}_p$ to hover in the region where $r_n = 1$, unless $z_n = 0$, in which case the necessary $\tilde{a}_p$ will drop to 0 (this situations occurs at the equilibrium point along the $+x$ axis, which lies in the asteroid's shadow). We can understand how $\tilde{a}_p$ approaches ∞ as r_n goes to 1 by inspection of Eq. (25); as r_n approaches 1, $\tan\alpha$ tends to ∞, which implies that α goes to $\pi/2$ as we approach this radius. As this case occurs, we lose the net solar radiation pressure force on the sail, although we still must generate force to make the sail hover. Thus, a larger sail acceleration is needed to counter this effect, which leads to infinite values at $r_n = 1$. We can also see from Eq. (30) that it is impossible to hover outside of the Hill radius, $r_n = 1$, as the tidal and SRP forces then cause the sail to escape. Conversely, on the asteroid day side ($\pi/2 < \theta \le \pi$), r_n must be greater than 1 to achieve equilibrium because $\tan\theta$ is negative in this region. The situation is reversed here because the sail cannot hover close to the asteroid, but must maintain some distance from it. Again, as r_n approaches 1, the necessary acceleration becomes large, for reasons similar as described.

Orbital Constraints and Dynamics

We now explore orbital options for the sail about the asteroid. We look for orbits that are stable in the sense that they neither impact the asteroid nor escape. Here we use results from previous investigations to identify a family of stable orbits for a solar sail.[7–9] There are constraints on the orbit geometry and orbit size (as a function of the sail acceleration) for these trajectories to be feasible. These constraints are presented as a function of basic asteroid parameters and heliocentric orbit. When these constraints are met and the orbits are feasible, they have a number of features that make them attractive, including better asteroid coverage and nearly trivial station-keeping costs. In this section we will assume $\alpha = \phi = 0$, so that the sail is face-on to the sun. For this case, then, $\boldsymbol{a} = [a_p \;\; 0 \;\; 0]$.

Sail Constraints for Bound Orbits

A sufficient condition for the orbit semimajor axis of a spacecraft subject to large solar radiation pressure perturbations to be orbitally bound to an asteroid can be derived to be[10,11]

$$a_{sc} < (\tilde{R}/4)\sqrt{\mu/a_{p0}} \tag{52}$$

where a_{sc} is the orbit semimajor axis and $\tilde{R}$ is the asteroid–sun distance in AU. This equation places a restriction on the size of an orbit as a function of the asteroid mass, distance from the sun, and sail acceleration. Spacecraft with semimajor axes greater than this limit are subject to being stripped from the asteroid and injected into a heliocentric orbit.

Defining the normalized semimajor axis $\tilde{a}_{sc} = a_{sc}/r_0$, where r_0 is the mean asteroid radius, we can derive the maximum sail acceleration for feasible orbital operations for the case when $\tilde{a}_{sc} = 1$:

$$a^M_{p0} = (\tilde{R}^2/16)\left(\mu/r_0^2\right) \tag{53}$$

This equation is clearly an upper bound, whereas, in general, we wish to limit the sail's acceleration as a function of the orbit semimajor axis $\tilde{a}_{sc}$:

$$a_{p0} < \left(1/\tilde{a}_{sc}^2\right)a^M_{p0} \tag{54}$$

where $\tilde{a}_{sc} > 1$, in general. Some characteristic values of the parameter a^M_{p0} are shown for different asteroids in Table 1. These values indicate that smaller asteroids will require low values of sail acceleration for orbital options to be feasible about them.

For a sail orbit that is bound, according to the preceding expression, it has been found[9] that the semimajor axis of the orbit is constant, on average. The other mean orbit elements are not constant, however and, in general, will have large secular variations over time. We confirm these findings in our numerical integrations as well.

Sail Orbit Dynamics About Asteroids

Assuming we have a solar sail with sail acceleration less than the bound given in Eq. (54), it becomes feasible to discuss orbital operations of the sail about the asteroid. The general orbital dynamics of such a bound, highly perturbed orbit are discussed in greater detail in Refs. 7–9. In Ref. 9, a particular class of stable orbits in the highly perturbed SRP problem was identified that is particularly well suited to solar sails. These orbits lie in the plane perpendicular to the asteroid–sun line, nominally have their periapsis aligned 90 deg above or below the orbit plane, and have their eccentricity chosen according to the equation

$$e = \cos\gamma \tag{55}$$

$$\tan\gamma = \tfrac{3}{2}a_{p0}R_0^2\sqrt{a_{sc}/P\mu\mu_{sun}} \tag{56}$$

where R_0 is one astronomical unit in kilometers and P is the orbit parameter of the asteroid, equal to the heliocentric radius for a circular orbit. We can rewrite this result as

$$\tan\gamma = \sqrt{\tilde{a}_{sc}}a_{p0}\Big/a^m_{p0} \tag{57}$$

$$a^m_{p0} = \tfrac{2}{3}\sqrt{\mu_{sun}\Big/R_0^3}\sqrt{\tilde{R}\mu/r_0} \tag{58}$$

$$a^m_{p0} \sim 1.33 \times 10^{-7}\sqrt{\tilde{R}\mu/r_0} \tag{59}$$

where $\tilde{R}$ is the asteroid–sun distance in astronomical units. Some characteristic values of a^m_{p0} for some select asteroids are shown in Table 1. From these values we note that $\tan\gamma \gg 1$, in general, indicating that the stable orbits will have near zero eccentricity.

Shown in Figs. 3–7 is a sample of numerically integrated sail trajectories about an asteroid, with the sail placed in a stable orbit as described. Note that the integration occurs in the frame rotating with the asteroid–sun line. This condition implies that these orbits are sun-synchronous in that they remain fixed in the sun plane of sky as shown in Fig. 4. We also note that the trajectory oscillates about a circular orbit in general, but is stable, as shown in Fig. 5.

These trajectories were calculated using the ode45 algorithm from MATLAB® (The MathWorks, Inc.) on the state equations taken from the equations of motion. A relative tolerance of 10^{-6} and an absolute tolerance of 10^{-8} was used each time. Each trajectory was computed over a different time interval for the sake of clarity in the image.

We can extend the analytical solution of the sail trajectory about the asteroid beyond this simple circular orbit, relying on an analytical solution to the averaged solar radiation pressure problem formulated by Richter and Keller.[8] In their paper, they find the averaged angular momentum and periapsis vector of the orbit as a function of asteroid true anomaly with respect to the sun. Taking this general solution, we specialize it to our particular case by assuming that the

perturbation angle $\gamma \to \pi/2$. We then find the angular momentum vector and periapsis vector to be[8]

$$\boldsymbol{H} = \sqrt{\mu a_{sc}} \begin{bmatrix} C_1 \\ C_2 \sin(N) + C_3 \cos(N) \\ C_5 \cos(N) - C_6 \sin(N) \end{bmatrix} \tag{60}$$

$$e = -\begin{bmatrix} C_4 \\ C_5 \sin(N) + C_6 \cos(N) \\ C_2 \cos(N) - C_3 \sin(N) \end{bmatrix} \tag{61}$$

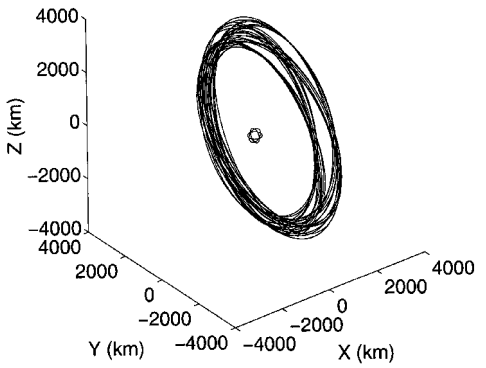

Fig. 3 Integrated orbit for a sail about Vesta using orbital elements $a_{sc} = 13r_0$, $e = \omega = \nu_0 = 0$, and $i = \Omega_0 = \pi/2$, and parameters $r_0 = 244.27$ km, $0 < t < 116$ days, and $a_{p_0} = 1$ mm/s^2; spacecraft position units are in kilometers, trajectory is shown in the coordinate system rotating with the asteroid about the sun.

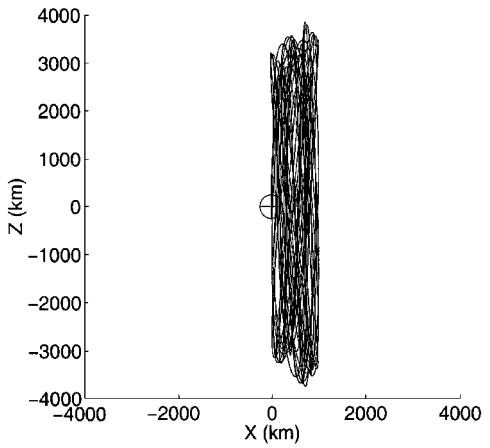

Fig. 4 Integrated orbit for a sail about Vesta in the *xz* plane using orbital elements and parameters of Fig. 3; trajectory is shown in the coordinate system rotating with the asteroid about the sun.

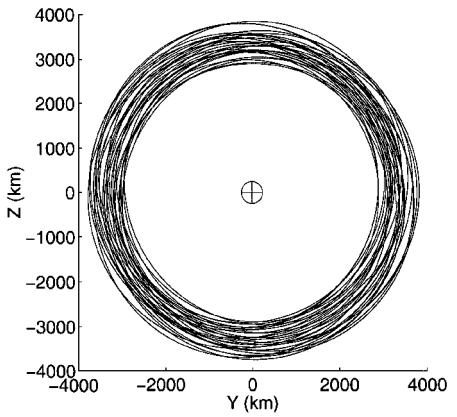

Fig. 5 Integrated orbit for a sail about Vesta in the *yz* plane using orbital elements and parameters of Fig. 3; trajectory is shown in the coordinate system rotating with the asteroid about the sun.

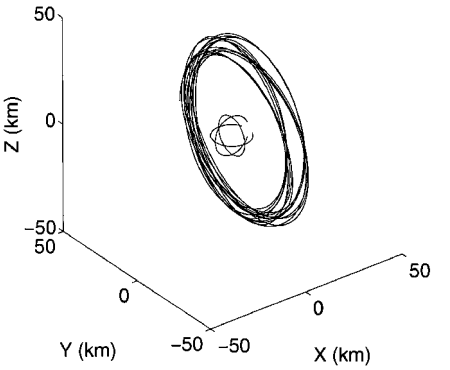

Fig. 6 Integrated orbit for a sail about Eros with $a_{sc} = 4r_0$: e, i, ω, Ω_0, and ν_0 the same as in Fig. 3; $r_0 = 8.87$ km, $0 < t < 12$ days, and $a_{p_0} = 0.1$ mm/s^2; trajectory is shown in the coordinate system rotating with the asteroid about the sun.

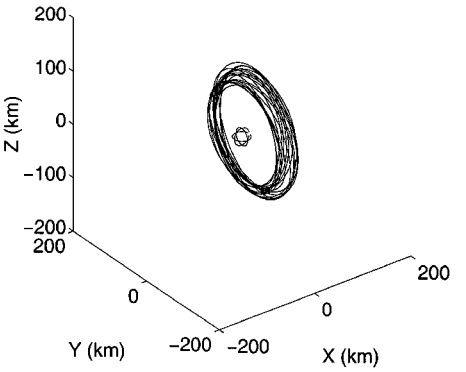

Fig. 7 Integrated orbit for a sail about Ida with $a_{sc} = 6r_0$: e, i, ω, Ω_0, and ν_0 the same as in Fig. 3; $r_0 = 15.65$ km, $0 < t < 24$ days, and $a_{p_0} = 0.5$ mm/s^2; trajectory is shown in the coordinate system rotating with the asteroid about the sun.

where N is an angle proportional to the asteroid true anomaly about the sun. The constants C_i can be related to the initial osculating orbital elements of the sail orbit as

$$C_1 = \sqrt{1 - e^2} \sin i \sin \tilde{\Omega} \tag{62}$$

$$C_2 = -e \sin i \sin \omega \tag{63}$$

$$C_3 = -\sqrt{1 - e^2} \sin i \cos \tilde{\Omega} \tag{64}$$

$$C_4 = -e[\cos \tilde{\Omega} \cos \omega - \cos i \sin \tilde{\Omega} \sin \omega] \tag{65}$$

$$C_5 = \sqrt{1 - e^2} \cos i \tag{66}$$

$$C_6 = -e[\sin \tilde{\Omega} \cos \omega + \cos i \cos \tilde{\Omega} \sin \omega] \tag{67}$$

where e is the orbit eccentricity, i is the orbit inclination measured from the asteroid ecliptic plane, $\tilde{\Omega}$ is the orbit longitude of the ascending node measured from the sun–asteroid line, and ω is the argument of periapsis. From this solution it is possible to evaluate the evolution of the mean orbit elements as a function of $N \sim nt/\cos\gamma$, where n is the asteroid's mean motion about the sun, t is time, and γ is the perturbation angle again. We note that for $0 < \pi/2 - \gamma \ll 1$, which is our case, the angle N will increase very rapidly with time, indicating that the mean solutions will oscillate rapidly. This result is not necessarily desirable, as can be seen if we take as initial conditions $i = 0$ and $e = 0$, giving $C_1 = C_2 = C_3 = C_4 = C_6 = 0$ and $C_5 = 1$. The solution then becomes

$$e = |\sin(N)| \tag{68}$$

$$\omega = \pm\pi/2 \tag{69}$$

$$i = 0 \tag{70}$$

meaning that the orbit will remain in the ecliptic plane, and the eccentricity will repeatedly pass through a value of unity, eventually causing the sail to impact on the asteroid surface.

If instead we take initial conditions $i = \pi/2$, $e = 0$, and $\tilde{\Omega} = \tilde{\Omega}_0$, we find the solution

$$i = \pi/2 \tag{71}$$

$$\omega = \pm\pi/2 \tag{72}$$

$$e = |\cos\tilde{\Omega}_0||\sin(N)| \tag{73}$$

$$\tan\tilde{\Omega} = \tan\tilde{\Omega}_0/\cos(N) \tag{74}$$

Now the orbit plane remains normal to the asteroid ecliptic, the longitude of the ascending node varies between $\tilde{\Omega}_0 \le \tilde{\Omega} \le \pi - \tilde{\Omega}_0$, and the eccentricity varies between $0 \le e \le |\cos\tilde{\Omega}_0|$. These conditions are a potentially useful generalization of the stable circular orbit discussed earlier that allows the orbit plane to move out of the sun plane of sky while bounding the maximum value of eccentricity. In Fig. 8 we show another plot of a numerically integrated orbit that shows this characteristic solution. Note that, even though the oscillations in mean elements occur rapidly, it is not valid to average over them because the amplitude of the oscillations are large. In Fig. 9, we show how eccentricity varies with $\tilde{\Omega}$. This particular type of orbit allows the asteroid to be imaged from a range of phase angles.

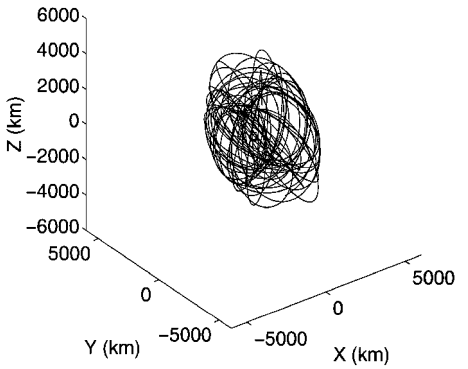

Fig. 8 Integrated orbit for a sail about Vesta with a_{sc}, e, i, ω, ν_0, and a_{p_0} the same as in Fig. 3; Ω_0 = 45 deg and $0 < t < 116$ days; trajectory is shown in the scoordinate system rotating with the asteroid about the sun.

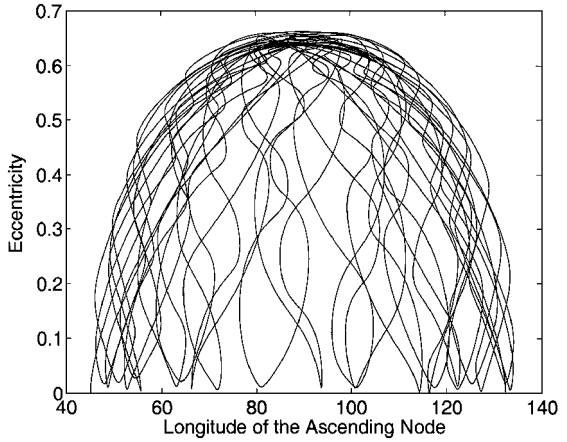

Fig. 9 Eccentricity vs longitude of the ascending node relative to the sun–asteroid line for the orbit about Vesta depicted in Fig. 8.

This family of solutions provides a viable family of stable, sun-synchronous sail orbits about asteroids that require no active control to maintain and that allows the sail to view the asteroid over a range of phase angles for long periods of time. Because these orbits are stable, we do not need to apply any closed-loop control to stabilize the sail, which implies that the orbital operations will be safer and require less operational effort.

For future studies, it will be of interest to include the effects of an asteroid's nonspherical gravity field in the sail orbital dynamics. The effects of these perturbations are difficult to predict but could lead to situations where the orbital dynamics become significantly modified, perhaps leading to the destabilization of the orbital motion in some cases. In general, however, it is possible to mitigate the effects of the asteroid gravity field on orbital motion by moving to a larger semimajor axis, although this will further constrain the sail acceleration [Eq. (54)]. In the simplest case, the effect of the oblateness of the asteroid will cause the orbit plane to precess about the asteroid pole. This precession will fight with the precession of the orbit plane caused by the solar radiation pressure, with the net effect of this interaction being an open question for future study.

Conclusions

We have shown that both hovering and orbital options are available with a solar sail spacecraft operating in close proximity to a spherical asteroid in a circular orbit. There are a continuum of hovering positions available near the asteroid. These hovering points depend on sail attitude, asteroid mass, and the acceleration of the sail. For a given distance from the asteroid and sail acceleration, the sail attitude can be determined to maintain that position for extended periods of time.

It has also been shown that several orbital options are available that offer good coverage of the asteroid and that neither impact the surface nor escape. These orbits are stable and sun synchronous. A sail could maintain orbit for extended periods of time in such an orbit. Some asteroids (such as Eros) require small sail accelerations for orbital operations to be feasible. In such cases as these, where it may be necessary to reduce the sail acceleration, we can make adjustments with trims in the sail area. With the possible exception of spin-stabilized sails, the deployment mechanism could be reversed so that the sail could be partially refurled. In this way we could decrease the sail area and thereby decrease a_p, making orbital operations about smaller asteroids possible.

Solar sails offer the advantage that long-duration missions can be planned, visiting several solar system objects, without the spacecraft mass and complexity involved with conventional propulsion and fuel supply. For example, after one asteroid has been investigated, the spacecraft is capable of escaping from orbit, in principle under sail propulsion alone, and traveling to another asteroid or returning to Earth. This capability offers the potential for low-cost and flexible solar system exploration.

Acknowledgments

Research at the University of California, San Diego, was supported by the National Science Foundation, NSF-OPP 98 06941. Research at the University of Michigan was supported by the Telecommunications and Missions Operations Directorate Technology Program by a grant from the Jet Propulsion Laboratory, California Institute of Technology, which is under contract with NASA.

References

[1]McInnes, C. R., *Solar Sailing: Technology, Dynamics and Mission Applications,* Praxis, Chichester, England, U.K., 1999, pp. 1–55.

[2]McInnes, C. R., McDonald, A. J. C., Simmons, J. F. L., and MacDonald, E. W., "Solar Sail Parking in Restricted Three-Body Systems," *Journal of Guidance, Control, and Dynamics*, Vol. 17, No. 2, 1994, pp. 399–406.

[3]McInnes, C. R., "Artificial Lagrange Points for a Partially Reflecting Flat Solar Sail," *Journal of Guidance, Control, and Dynamics*, Vol. 22, No. 1, 1999, pp. 185–187.

[4]Scheeres, D. J., "The Restricted Hill Four-Body Problem with Applications to the Earth–Moon–Sun System," *Celestial Mechanics and Dynamical Astronomy*, Vol. 70, No. 2, 1998, pp. 75–98.

[5]Scheeres, D. J., and Marzari, F., "Spacecraft Dynamics Far from a Comet," *Journal of Astronautical Sciences* (submitted for publication).

[6]McInnes, A. I., "Strategies for Solar Sail Mission Design in the Circular Restricted Three-Body Problem," M.S. Thesis, School of Aeronautics and Astronautics, Purdue Univ., West Lafayette, IN, Aug. 2000.

[7]Mignard, F., and Henon, M., "About an Unsuspected Integrable Problem," *Celestial Mechanics*, Vol. 33, No. 2, 1984, pp. 239–250.

[8]Richter, K., and Keller, H. U., "On the Stability of Dust Particle Orbits Around Cometary Nuclei," *Icarus*, Vol. 114, No. 2, 1995, pp. 355–371.

[9]Scheeres, D. J., "Satellite Dynamics About Small Bodies: Averaged Solar Radiation Pressure Effects," *Journal of the Astronautical Sciences*, Vol. 47, Nos. 1 and 2, 1999, pp. 25–46.

[10]Hamilton, D. P., and Burns, J. A., "Orbital Stability Zones About Asteroids II. The Destabilizing Effects of Eccentricities and of Solar Radiation," *Icarus*, Vol. 96, No. 1, 1992, pp. 43–64.

[11]Scheeres, D. J., "Analysis of Orbital Motion Around 433 Eros," *Journal of the Astronautical Sciences*, Vol. 43, No. 4, 1995, pp. 427–452.

A. C. Tribble
Associate Editor